USING COUPLED OSCILLATORS TO MODEL THE SINO-ATRIAL NODE IN THE HEART

A Thesis

Presented to the Faculty of the Graduate School

of Cornell University

in Partial Fulfillment of the Requirements for the Degree of

Master of Science

by

Marqui Johnson

August 2005

TABLE OF CONTENTS

LIST OF FIGURES

ABSTRACT

The Sinoatrial (SA) node (i.e. pacemaker) is the region of the heart that initiates a regular heartbeat. Studies have shown that the SA node is composed of self-oscillatory cells that create an electrical impulse. Although individual oscillatory cells may have different frequencies, as a whole the SA node normally releases a periodic collective impulse which travels to other parts of the heart.

In this thesis we construct a simple model of the pacemaker consisting of five phase-only oscillators. Then through the use of stability analysis we determine what conditions are necessary for a stable system. Further, we find an analytic expression for the boundary of a region in a parameter space which contains the stable solutions.

Lastly, we devise another model of the SA node which consists of three Fitzhugh-Nagumo oscillators. We offer a preliminary study of this model in which we analyze the dynamics of a Fitzhugh-Nagumo oscillator using three different methods. The methods are: 1)Poincaré-Lindstedt, 2)Fast-Slow approximation, and 3)Numerical Simulation. We compare the results of each method graphically and determine which is best for implementing our model.

Chapter 1

The Five Cell Model

1.1 Introduction (Keener and Sneyd p.389)

The Sinoatrial Node (SA Node) is a clump of self-oscillatory cells located on the right atrium near the superior vena cava. It is the SA Node which initiates the stimulus for pacemaking activity. These cells fire regularly, initiating electronic potentials. The pacemaker impulse from the SA Node spreads through both atria as a wave of depolarization. These regular impulses cause the atria to contract. Once stimulated the Atrioventricular Node (AV Node) transmits the electrical stimulus down the Right and Left Bundle Branches to stimulate both ventricles. The impulse quickly spreads to both ventricles to initiate their simultaneous depolarization. The result is a normal rhythm of the heart often referred to as regular.

1.2 Model

Normally, SA nodal cells are not identical or synchronous in their firing (i.e., firing all at once), but they are phase locked, meaning that during each cycle, each cell fires once and there is a regular pattern to the firing of the cells. Under what conditions does this regular pattern of firing become unstable?

1.2.1 Assumptions

1. We suppose that the SA node is composed of self-oscillatory cells coupled together in a network.

2. We assume that the cells each contribute equally to the normal performance.

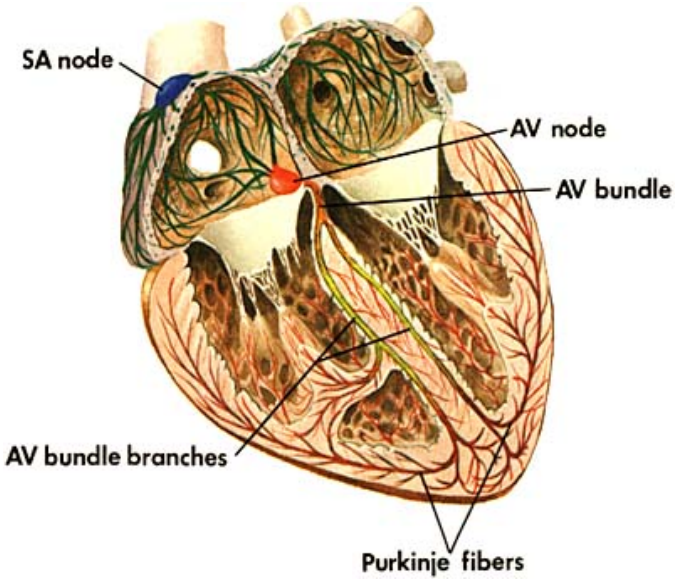

Figure 1.1: Location of the SA node.
Image courtesy of biology.about.com/library/organs/heart/blsinoatrialnode.htm

3. The cells fire rhythmically which we may interpret as periodic.

4. Because the cells are self-oscillatory we assume that each cell has its own frequency that is not necessarily equal to another cell's frequency.

First, we begin by discussing the model of a single oscillator. From our assumption that cells fire periodically, we will define θ as the phase of a cell. Then $\theta' = \omega$, the oscillator's frequency. We can model the motion of θ around a closed circular path since we know after a certain period the phase repeats its previous cycle. The "clump" will be defined as a collection of five cells connected via nearest neighbor coupling meaning that each cell is influenced by the cell adjacent to it (see Fig.2).

This coupling is represented mathematically as

$$\theta_0' = \omega_0 + \alpha[\sin(\theta_1 - \theta_0)$$

.

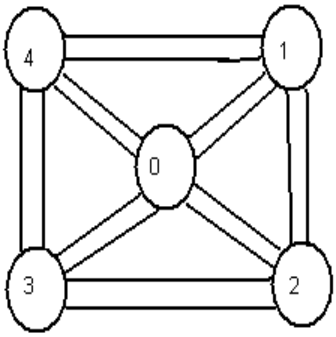

Figure 1.2: The model of the clump where each cell is coupled to the cell adjacent to it.

$$+\sin(\theta_2-\theta_0)+\sin(\theta_3-\theta_0)+\sin(\theta_4-\theta_0)] \tag{1.1}$$

$$\theta_1' = \omega_1+\alpha[\sin(\theta_4-\theta_1)+\sin(\theta_2-\theta_1)+\sin(\theta_0-\theta_1)] \tag{1.2}$$

$$\theta_2' = \omega_2+\alpha[\sin(\theta_1-\theta_2)+\sin(\theta_3-\theta_2)+\sin(\theta_0-\theta_2)] \tag{1.3}$$

$$\theta_3' = \omega_3+\alpha[\sin(\theta_2-\theta_3)+\sin(\theta_4-\theta_3)+\sin(\theta_0-\theta_3)] \tag{1.4}$$

$$\theta_4' = \omega_4+\alpha[\sin(\theta_3-\theta_4)+\sin(\theta_1-\theta_4)+\sin(\theta_0-\theta_4)] \tag{1.5}$$

We are able to use the same coupling coefficient, α , in each equation because of Assumption 2. We chose the sine function for coupling because 1.)the phases are periodic, 2.) any periodic function can be represented in a Fourier Series of which we are taking the first term, and 3.) for our model we require that if the θ_i's are equal, the function of the differences should equal zero.

For mathematical simplicity we define $\Phi_i = \theta_i - \theta_0$, whereupon also $\Phi_i' = \theta_i' - \theta_0'$ for $i = 1, 2, 3, 4$. Eqs.(2.11)-(2.5) become:

$$\begin{aligned}
\Phi_1' &= \omega_1 - \omega_0 + \alpha[\sin(\Phi_2 - \Phi_1) \\
&\quad + \sin(\Phi_4 - \Phi_1) - 2\sin(\Phi_1) - \sin(\Phi_2) - \sin(\Phi_3) - \sin(\Phi_4)] \qquad (1.6)\\
\Phi_2' &= \omega_2 - \omega_0 + \alpha[\sin(\Phi_3 - \Phi_2) \\
&\quad + \sin(\Phi_1 - \Phi_2) - \sin(\Phi_1) - 2\sin(\Phi_2) - \sin(\Phi_3) - \sin(\Phi_4)] \qquad (1.7)\\
\Phi_3' &= \omega_3 - \omega_0 + \alpha[\sin(\Phi_4 - \Phi_3) \\
&\quad + \sin(\Phi_2 - \Phi_3) - \sin(\Phi_1) - \sin(\Phi_2) - 2\sin(\Phi_3) - \sin(\Phi_4)] \qquad (1.8)\\
\Phi_4' &= \omega_4 - \omega_0 + \alpha[\sin(\Phi_1 - \Phi_4) \\
&\quad + \sin(\Phi_3 - \Phi_4) - \sin(\Phi_1) - \sin(\Phi_2) - \sin(\Phi_3) - 2\sin(\Phi_4)] \qquad (1.9)
\end{aligned}$$

The previous substitution allows us to reduce the number of equations from five to four. We are interested in conditions such that the cells are all phase-locked. Mathematically, this means that the phase differences are constant. If $\Phi_i = c_i$, a constant, then $\Phi_i' = 0$. Solving for Φ_i when Φ_i' equals zero will give us the equilibria for which the cells are phase-locked. With $\Phi_i' = 0$ and substituting $\Omega_i = \frac{\omega_0 - \omega_i}{\alpha}$, we get the following equations,

$$\begin{aligned}
\Omega_1 &= \sin(\Phi_2 - \Phi_1) + \sin(\Phi_4 - \Phi_1) \\
&\quad -2\sin(\Phi_1) - \sin(\Phi_2) - \sin(\Phi_3) - \sin(\Phi_4)) \qquad (1.10)\\
\Omega_2 &= \sin(\Phi_3 - \Phi_2) + \sin(\Phi_1 - \Phi_2) \\
&\quad - \sin(\Phi_1) - 2\sin(\Phi_2) - \sin(\Phi_3) - \sin(\Phi_4)) \qquad (1.11)\\
\Omega_3 &= \sin(\Phi_4 - \Phi_3) + \sin(\Phi_2 - \Phi_3) \\
&\quad - \sin(\Phi_1) - \sin(\Phi_2) - 2\sin(\Phi_3) - \sin(\Phi_4)) \qquad (1.12)\\
\Omega_4 &= \sin(\Phi_1 - \Phi_4) + \sin(\Phi_3 - \Phi_4)
\end{aligned}$$

$$-\sin(\Phi_1) - \sin(\Phi_2) - \sin(\Phi_3) - 2\sin(\Phi_4)) \tag{1.13}$$

1.3 Numerical Solutions

To find the phase-locked solutions we must determine the equilibria of Eqs.(1.10)-(1.13). Once the equilibria have been found the next step is to determine their stability. We can use Newton-Raphson or the Bisection method to find numerical solutions for the values of the equilibria given the values of the frequency differences,Ω_i. Instead we choose to use an inverse approach. A program was written that picked random numbers for each Φ_i allowing for values to be computed for each frequency difference, Ω_i. Simultaneously, the stability of each equilibrium point was determined. A stability matrix was created by linearizing Eqs.(2.6)-(1.9) about an equilibrium point:

$$\begin{pmatrix} A_{11} & A_{12} & A_{13} & A_{14} \\ A_{21} & A_{22} & A_{23} & A_{24} \\ A_{31} & A_{32} & A_{33} & A_{34} \\ A_{41} & A_{42} & A_{43} & A_{44} \end{pmatrix} \tag{1.14}$$

where

$$A_{11} = -\cos(\Phi_2 - \Phi_1) - \cos(\Phi_4 - \Phi_1) - 2\cos(\Phi_1) \tag{1.15}$$

$$A_{12} = \cos(\Phi_2 - \Phi_1) - \cos(\Phi_2) \tag{1.16}$$

$$A_{13} = -\cos(\Phi_3) \tag{1.17}$$

$$A_{14} = \cos(\Phi_4 - \Phi_1) - \cos(\Phi_4) \tag{1.18}$$

$$A_{21} = \cos(\Phi_1 - \Phi_2) - \cos(\Phi_1) \tag{1.19}$$

$$A_{22} = -\cos(\Phi_3 - \Phi_2) - \cos(\Phi_1 - \Phi_2) - 2\cos(\Phi_2) \quad (1.20)$$

$$A_{23} = \cos(\Phi_3 - \Phi_2) - \cos(\Phi_3) \quad (1.21)$$

$$A_{24} = -\cos(\Phi_4) \quad (1.22)$$

$$A_{31} = -\cos(\Phi_1) \quad (1.23)$$

$$A_{32} = \cos(\Phi_2 - \Phi_3) - \cos(\Phi_2) \quad (1.24)$$

$$A_{33} = -\cos(\Phi_4 - \Phi_3) - \cos(\Phi_2 - \Phi_3) - 2\cos(\Phi_3) \quad (1.25)$$

$$A_{34} = \cos(\Phi_4 - \Phi_3) - \cos(\Phi_4) \quad (1.26)$$

$$A_{41} = \cos(\Phi_1 - \Phi_4) - \cos(\Phi_1) \quad (1.27)$$

$$A_{42} = -\cos(\Phi_2) \quad (1.28)$$

$$A_{43} = \cos(\Phi_3 - \Phi_4) - \cos(\Phi_3) \quad (1.29)$$

$$A_{44} = -\cos(\Phi_1 - \Phi_4) - \cos(\Phi_3 - \Phi_4) - 2\cos(\Phi_4) \quad (1.30)$$

and where the coefficients A_{ij} are evaluated at a given equilibrium point.

If the real parts of the eigenvalues of this matrix are negative, the equilibrium is stable. If there is at least one eigenvalue with a positive real part then the equilibrium is unstable. All of the stable Φ_i were stored and their respective Ω_i were plotted two at a time giving us six possible different plots. Unstable points were not plotted.

1.3.1 Numerical Results

After viewing all the possible combinations of the Ω_i plots we noticed there were essentially only two different plots - one representing adjacent cells and one for the non-adjacent cells (see Figs. 3 and 4). From Figs. 3 and 4 it is apparent that in order for the pacemaker to operate in a stable manner, the frequency differences, Ω_i, must be sufficiently small. Although the numerical results consist of discrete

points it is apparent from Figs. 3 and 4 that there is a smooth boundary between stable and unstable points. In what follows we obtain an approximation for this boundary.

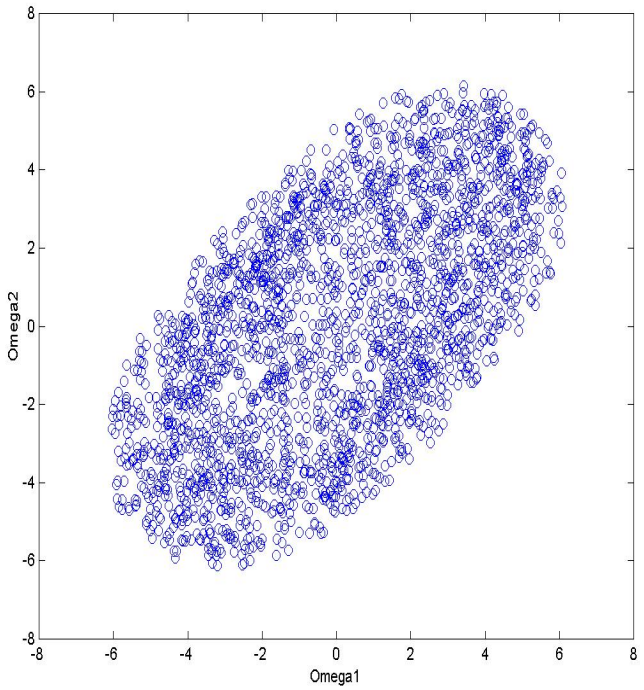

Figure 1.3: Stability plot for Ω_1 vs Ω_2. Represents two adjacent cells.

1.4 Perturbation Method

1.4.1 Scaling Equations with ϵ

The idea of the perturbation method is to obtain an approximate analytic solution to compare with the numerical solution described above. It is based on a known solution, namely that when all ω_i's are equal, i.e. $\Omega_i = 0$, an exact solution is

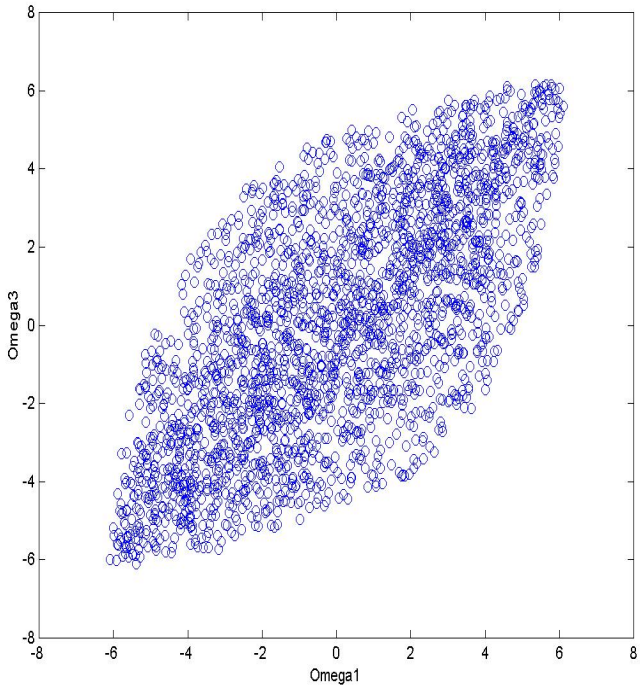

Figure 1.4: Stability plot for Ω_1 vs Ω_3. Represents two diagonal cells.

easily shown to be $\Phi_i = 0$. This solution is stable as can be seen from expression (1.14) which becomes for $\Phi_i = 0$

$$\begin{pmatrix} -4 & 0 & -1 & 0 \\ 0 & -4 & 0 & -1 \\ -1 & 0 & -4 & 0 \\ 0 & -1 & 0 & -4 \end{pmatrix} \tag{1.31}$$

which has eigenvalues, -3,-3,-5,-5. The perturbation method is based on perturbing off of this special solution.

We proceed by scaling Ω_i and Φ_i with small ϵ: $\Omega_i = \epsilon\hat{\Omega}_i$ and $\Phi_i = \epsilon\hat{\Phi}_i$. We substitute our new Ω_i and Φ_i into equations (1.10)-(1.13):

$$\begin{aligned}
\epsilon\hat{\Omega}_1 &= \sin(\epsilon\hat{\Phi}_2 - \epsilon\hat{\Phi}_1) + \sin(\epsilon\hat{\Phi}_4 - \epsilon\hat{\Phi}_1) \\
&\quad -2\sin(\epsilon\hat{\Phi}_1) - \sin(\epsilon\hat{\Phi}_2) - \sin(\epsilon\hat{\Phi}_3) - \sin(\epsilon\hat{\Phi}_4)) \qquad (1.32) \\
\epsilon\hat{\Omega}_2 &= \sin(\epsilon\hat{\Phi}_3 - \epsilon\hat{\Phi}_2) + \sin(\epsilon\hat{\Phi}_1 - \epsilon\hat{\Phi}_2) \\
&\quad -\sin(\epsilon\hat{\Phi}_1) - 2\sin(\epsilon\hat{\Phi}_2) - \sin(\epsilon\hat{\Phi}_3) - \sin(\epsilon\hat{\Phi}_4)) \qquad (1.33) \\
\epsilon\hat{\Omega}_3 &= \sin(\epsilon\hat{\Phi}_4 - \epsilon\hat{\Phi}_3) + \sin(\epsilon\hat{\Phi}_2 - \epsilon\hat{\Phi}_3) \\
&\quad -\sin(\epsilon\hat{\Phi}_1) - \sin(\epsilon\hat{\Phi}_2) - 2\sin(\epsilon\hat{\Phi}_3) - \sin(\epsilon\hat{\Phi}_4)) \qquad (1.34) \\
\epsilon\hat{\Omega}_4 &= \sin(\epsilon\hat{\Phi}_1 - \epsilon\hat{\Phi}_4) + \sin(\epsilon\hat{\Phi}_3 - \epsilon\hat{\Phi}_4) \\
&\quad -\sin(\epsilon\hat{\Phi}_1) - \sin(\epsilon\hat{\Phi}_2) - \sin(\epsilon\hat{\Phi}_3) - 2\sin(\epsilon\hat{\Phi}_4)) \qquad (1.35)
\end{aligned}$$

We Taylor expand Eqs.(1.32)-(1.35) for small ϵ and neglect terms of $O(\epsilon^2)$. The resulting equations may be solved for the $\hat{\Phi}_i$, giving

$$\hat{\Phi}_1 = \frac{4\hat{\Omega}_1 - \hat{\Omega}_3}{15} \qquad (1.36)$$

$$\hat{\Phi}_2 = \frac{4\hat{\Omega}_2 - \hat{\Omega}_4}{15} \qquad (1.37)$$

$$\hat{\Phi}_3 = \frac{\hat{\Omega}_1 - 4\hat{\Omega}_3}{15} \qquad (1.38)$$

$$\hat{\Phi}_4 = \frac{\hat{\Omega}_2 - 4\hat{\Omega}_4}{15} \qquad (1.39)$$

.

1.4.2 Stability

Given an equilibrium point, the question of its stability is this: If we deviate from it, will we return to the equilibrium or continue to move away? If we return to the point this means that the equilibrium is stable, whereas if we move away, it is unstable. In our case, the sinoatrial node may incur small deviations from its regular

pattern of beating but will usually return to a steady beat. On some occasions, the deviation may be too great, causing the pacemaker to become irregular. We now have $\hat{\Phi} = \hat{\Phi}_i^\star + u_i$, where $\hat{\Phi}_i^\star$ is our known solution, and where u_i is a small deviation. We substitute $\Phi_i = \epsilon\hat{\Phi}_i = \epsilon(\hat{\Phi}_i^\star + u_i)$ into equations (2.6) - (1.9) and linearize them to get a stability matrix. The result is as follows

$$\begin{pmatrix} u_1 \\ u_2 \\ u_3 \\ u_4 \end{pmatrix}' = \begin{pmatrix} A_{11} & A_{12} & A_{13} & A_{14} \\ A_{21} & A_{22} & A_{23} & A_{24} \\ A_{31} & A_{32} & A_{33} & A_{34} \\ A_{41} & A_{42} & A_{43} & A_{44} \end{pmatrix} \begin{pmatrix} u_1 \\ u_2 \\ u_3 \\ u_4 \end{pmatrix} \tag{1.40}$$

where

$$A_{11} = -\cos(\epsilon\hat{\Phi}_2^\star - \epsilon\hat{\Phi}_1^\star) - \cos(\epsilon\hat{\Phi}_4^\star - \epsilon\hat{\Phi}_1^\star) - 2\cos(\epsilon\hat{\Phi}_1^\star) \tag{1.41}$$

$$A_{12} = \cos(\epsilon\hat{\Phi}_2^\star - \epsilon\hat{\Phi}_1^\star) - \cos(\epsilon\hat{\Phi}_2^\star) \tag{1.42}$$

$$A_{13} = -\cos(\epsilon\hat{\Phi}_3^\star) \tag{1.43}$$

$$A_{14} = \cos(\epsilon\hat{\Phi}_4^\star - \epsilon\hat{\Phi}_1^\star) - \cos(\epsilon\hat{\Phi}_4^\star) \tag{1.44}$$

$$A_{21} = \cos(\epsilon\hat{\Phi}_1^\star - \epsilon\hat{\Phi}_2^\star) - \cos(\epsilon\hat{\Phi}_1^\star) \tag{1.45}$$

$$A_{22} = -\cos(\epsilon\hat{\Phi}_3^\star - \epsilon\hat{\Phi}_2^\star) - \cos(\epsilon\hat{\Phi}_1^\star - \epsilon\hat{\Phi}_2^\star) - 2\cos(\epsilon\hat{\Phi}_2^\star) \tag{1.46}$$

$$A_{23} = \cos(\epsilon\hat{\Phi}_3^\star - \epsilon\hat{\Phi}_2^\star) - \cos(\epsilon\hat{\Phi}_3^\star) \tag{1.47}$$

$$A_{24} = -\cos(\epsilon\hat{\Phi}_4^\star) \tag{1.48}$$

$$A_{31} = -\cos(\epsilon\hat{\Phi}_1^\star) \tag{1.49}$$

$$A_{32} = \cos(\epsilon\hat{\Phi}_2^\star - \epsilon\hat{\Phi}_3^\star) - \cos(\epsilon\hat{\Phi}_2^\star) \tag{1.50}$$

$$A_{33} = -\cos(\epsilon\hat{\Phi}_4^\star - \epsilon\hat{\Phi}_3^\star) - \cos(\epsilon\hat{\Phi}_2^\star - \epsilon\hat{\Phi}_3^\star) - 2\cos(\epsilon\hat{\Phi}_3^\star) \tag{1.51}$$

$$A_{34} = \cos(\epsilon\hat{\Phi}_4^\star - \epsilon\hat{\Phi}_3^\star) - \cos(\epsilon\hat{\Phi}_4^\star) \tag{1.52}$$

$$A_{41} = \cos(\epsilon\hat{\Phi}_1^\star - \epsilon\hat{\Phi}_4^\star) - \cos(\epsilon\hat{\Phi}_1^\star) \quad (1.53)$$

$$A_{42} = -\cos(\epsilon\hat{\Phi}_2^\star) \quad (1.54)$$

$$A_{43} = \cos(\epsilon\hat{\Phi}_3^\star - \epsilon\hat{\Phi}_4^\star) - \cos(\epsilon\hat{\Phi}_3^\star) \quad (1.55)$$

$$A_{44} = -\cos(\epsilon\hat{\Phi}_1^\star - \epsilon\hat{\Phi}_4^\star) - \cos(\epsilon\hat{\Phi}_3^\star - \epsilon\hat{\Phi}_4^\star) - 2\cos(\epsilon\hat{\Phi}_4^\star) \quad (1.56)$$

To determine the stability of the system, we need to determine the eigenvalues of the matrix in Eqs.(1.40). If they have negative real parts we have a stable equilibrium point. If there exists one eigenvalue with a positive real part it is unstable. Numerical simulation has shown that the eigenvalues of the stability matrix are real. For the transition between stable and unstable there will be an eigenvalue equal to zero. In order to determine the eigenvalues of any matrix, the formula $\det(I_n\lambda - A_n)$ is used. For a zero eigenvalue, $\lambda = 0$, we have det A = 0. After setting the determinant equal to zero we expanded it in a Taylor series in ϵ about zero. This yielded an expression with terms of order ϵ^2 and higher. Using only the ϵ^2 terms and setting them equal to zero, then dividing by ϵ^2, the result is the following quadratic polynomial in $\Omega_1, \Omega_2, \Omega_3, \Omega_4$:

$$\begin{aligned} f(\Omega_1,\Omega_2,\Omega_3,\Omega_4) = {} & 391(\Omega_4^2+\Omega_3^2+\Omega_2^2+\Omega_1^2) + \Omega_2\Omega_1) \\ & -144(\Omega_4\Omega_3 + \Omega_4\Omega_1 + \Omega_3\Omega_2 \\ & -368(\Omega_4\Omega_2 + \Omega_3\Omega_1) = 6750 \end{aligned} \quad (1.57)$$

.

1.4.3 Reduction of the Hypersurface to Canonical Form

In matrix form, $f(\Omega_1,\Omega_2,\Omega_3,\Omega_4) = \Omega^T A\Omega =$

$$\begin{pmatrix} \Omega_1 & \Omega_2 & \Omega_3 & \Omega_4 \end{pmatrix} \begin{pmatrix} 391 & -72 & -184 & -72 \\ -72 & 391 & -72 & -184 \\ -184 & -72 & 391 & -72 \\ -72 & -184 & -72 & 391 \end{pmatrix} \begin{pmatrix} \Omega_1 \\ \Omega_2 \\ \Omega_3 \\ \Omega_4 \end{pmatrix} \tag{1.58}$$

In order to diagonalize the matrix A, we set $\Omega = R\mu$:

$$\begin{pmatrix} \Omega_1 \\ \Omega_2 \\ \Omega_3 \\ \Omega_4 \end{pmatrix} = \begin{pmatrix} 1/2 & 1/2 & 0 & 1/\sqrt{2} \\ -1/2 & 1/2 & 1/\sqrt{2} & 0 \\ 1/2 & 1/2 & 0 & -1/\sqrt{2} \\ -1/2 & 1/2 & -1/\sqrt{2} & 0 \end{pmatrix} \begin{pmatrix} \mu_1 \\ \mu_2 \\ \mu_3 \\ \mu_4 \end{pmatrix} \tag{1.59}$$

where the columns of R are the orthonormal eigenvectors of A. Substituting (1.59) into (1.58) we get

$$f = \Omega^T A \Omega = \mu^T R^T A R \mu = \mu^T D \mu \tag{1.60}$$

where

$$D = \begin{pmatrix} 351 & 0 & 0 & 0 \\ 0 & 63 & 0 & 0 \\ 0 & 0 & 575 & 0 \\ 0 & 0 & 0 & 575 \end{pmatrix} \tag{1.61}$$

Using Eqs.(1.60), $f = 6750$ may be written in the form

$$\frac{\mu_1^2}{(4.3853)^2} + \frac{\mu_2^2}{(10.351)^2} + \frac{\mu_3^2}{(3.4262)^2} + \frac{\mu_4^2}{(3.4262)^2} = 1 \tag{1.62}$$

which is a four dimensional ellipsoid.

1.4.4 Projection onto $\Omega_1\Omega_2$ and $\Omega_1\Omega_3$-planes to Compare with Numerical Solutions

How can we compare our perturbation four dimensional solution with the two numerical plots Ω_1 vs. Ω_2 and Ω_1 vs. Ω_3, Figs. 2 and 3? First, we consider a simpler example. When we project a three dimensional surface onto a plane we recognize that the boundary of the resulting projection corresponds to the points where the normal vector to the surface is perpendicular to the normal vector to the plane. We extend this idea to four dimensions. Since our goal is to find the boundary equations of our numerical plots, we need to find the normal vector of $f(\Omega_1, \Omega_2, \Omega_3, \Omega_4)$. Say $\vec{n}$ is a vector normal to our ellipsoid. Then

$$\vec{n} = \nabla f \tag{1.63}$$

To project down onto the $\Omega_1 - \Omega_2$ plane, we want those points on the ellipsoid (1.62) for which ∇f is perpendicular to $\hat{e}_{\Omega_3}$ and $\hat{e}_{\Omega_4}$, since $\hat{e}_{\Omega_3}$ and $\hat{e}_{\Omega_4}$ are normal to the $\Omega_1 - \Omega_2$ plane.

So we have $\nabla f \cdot \hat{e}_{\Omega_i} = 0, i = 3, 4$. But

$$\nabla f = \frac{\partial f}{\partial \Omega_1}\hat{e}_{\Omega_1} + \frac{\partial f}{\partial \Omega_2}\hat{e}_{\Omega_2} + \frac{\partial f}{\partial \Omega_3}\hat{e}_{\Omega_3} + \frac{\partial f}{\partial \Omega_4}\hat{e}_{\Omega_4} \tag{1.64}$$

giving $\frac{\partial f}{\partial \Omega_i} = 0, i = 3, 4$ since

$$\hat{e}_{\Omega_i} \cdot \hat{e}_{\Omega_j} = \begin{cases} 1 & i = j \\ 0 & i \neq j \end{cases}$$

From Eqs.(1.57)

$$\frac{\partial f}{\partial \Omega_3} = -144(\Omega_4 + \Omega_2) + 782\Omega_3 - 368\Omega_1 \tag{1.65}$$

$$\frac{\partial f}{\partial \Omega_4} = 782\Omega_4 - 144(\Omega_3 + \Omega_1) - 368\Omega_2 \tag{1.66}$$

Setting $\frac{\partial f}{\partial \Omega_3} = 0$ and $\frac{\partial f}{\partial \Omega_4} = 0$, we can solve for Ω_3, Ω_4 in terms of Ω_1, Ω_2. Next we substitute these last expressions into Eqs.(1.57), giving an expression of the form

$$A\Omega_1^2 - B\Omega_1\Omega_2 + A\Omega_2^2 = 1$$

This last equation is an ellipse and may be plotted as in Fig. 5. We follow the same process for projection onto the $\Omega_1 - \Omega_3$ plane. See Fig. 6.

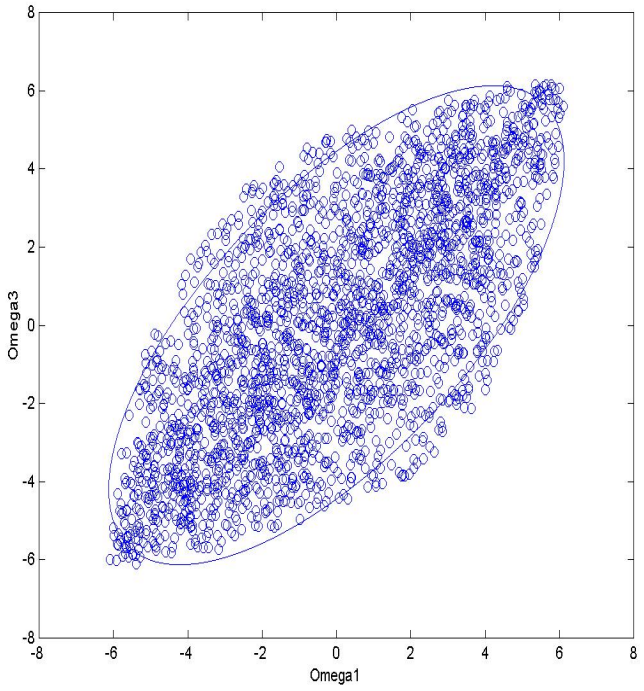

Figure 1.5: Stability plot for Ω_1 vs Ω_3 with boundary obtained from perturbation method.

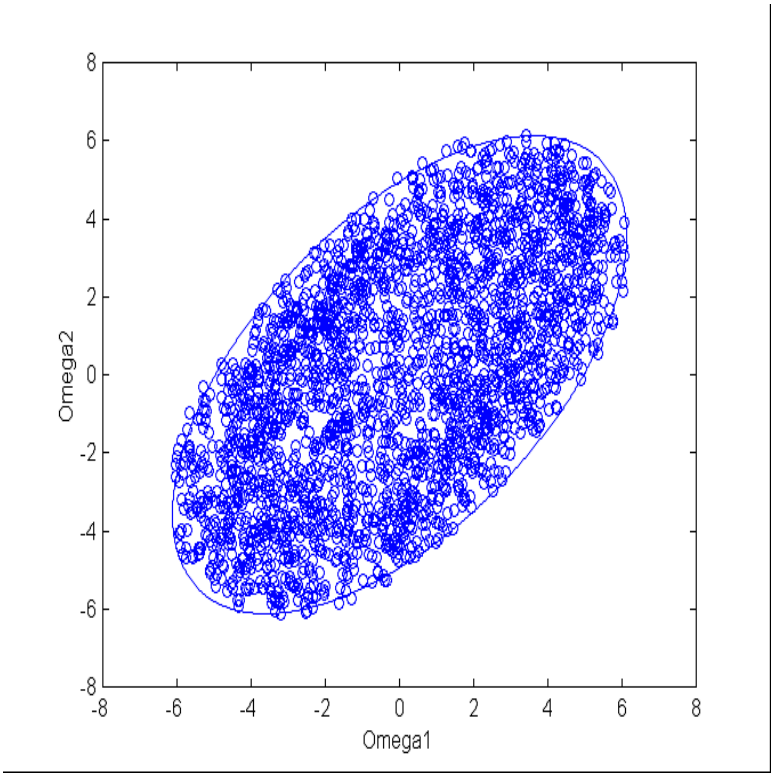

Figure 1.6: Stability plot for Ω_1 vs Ω_2 with boundary obtained from perturbation method.

1.5 Conclusions

In this investigation we used phase only oscillators to model our schematic Fig. (2.12) of the SA node. Our goal was to determine what conditions would allow our system to operate in a stable phase-locked mode. By design all the cells were connected via nearest neighbor coupling and are represented mathematically in Eqs.(2.11 - 2.5). For simplicity we defined $\Phi_i = \theta_i - \theta_0$ which allowed us to reduce the number of equations from five to four, Eqs.(2.11 - 2.5) and (2.6 - 1.9) respectively. We learned from *Keener and Sneyd* that under normal in vivo conditions, the cells are phase-locked. Mathematically, this means that the phase differences,Φ_i, are constant thus $\Phi_i' = 0$. Using this fact and substituting $\Omega_i = \frac{\omega_i - \omega_0}{\alpha}$, we arrived at Eqs.(1.10 - 1.13). It is interesting to note here that the stability of the system depended on the ratio of the difference of the cells'

uncoupled frequency differences, to the coupling strength. To analyze Eqs.(1.10)-(1.13) numerically, we employed an inverse approach. Using Matlab, random values for Φ_i were chosen allowing for values of Ω_i to be computed and their stabilities determined. The resulting stability plots are represented in Figs.(2.3)and(2.4).

To establish analytic approximations for the boundaries in Figs.(2.3)and(2.4) we used a perturbation method. We rescaled (1.10)-(1.13) by letting $\Omega_i = \epsilon\hat{\Omega}_i$ to get Eqs.(1.32)-(1.35). Then we defined a function f in terms of the Ω_i's,(1.57), as a result of the stability analysis. After reducing f to its canonical form, Eqs.(1.62), we found that it was a four dimensional ellipsoid. In order to compare this result to the numerical results in Figs.(2.3)and(2.4), we projected our four dimensional ellipsoid onto a plane. We were then able to produce quadratic equations in terms of Ω_1, Ω_2 and Ω_1, Ω_3 that yielded the results in Figs.(2.5)and(2.6). In our use of Taylor series expansion to derive f, we limited our approximation to terms of order ϵ^2. Consequently, our derived curves are close to the shape and size of the numerical results but not exact. Closer approximations can be obtained if more higher order terms are considered.

Finally, we conclude that if the Ω_i's are within the boundaries represented in Figs.(2.5)and(2.6) the pacemaker remains in a stable phase-locked state and a regular heartbeat is sustained.

Chapter 2

The Three Cell Model

2.1 Fitzhugh-Nagumo Equations

To further our analysis of the SA node, we would like to make a more representative model of the pacemaker. The literature reveals that not all the cells in the pacemaker have the same frequency as our previous model assumed. In fact, the periphery cells of the pacemaker have a higher frequency than the innermost cells (D. Cai 220). Also, the atrial tissue that surrounds the pacemaker is composed of cells that are not self-oscillatory. We will incorporate these findings into our new model using the Fitzhugh-Nagumo (FN) equations.

$$\epsilon \dot{v} = -v(v-\alpha)(v-1) - w, \ 0 < \epsilon \ll 1 \tag{2.1}$$

$$\dot{w} = v - w \tag{2.2}$$

In this model there is a range of values for the parameter α that gives oscillations. We propose a three cell model (Fig. 1) in which cell 1 and cell 2 are self-oscillatory to represent pacemaker cells, and cell 3 is not self-oscillatory to represent atrial tissue. Cell 2 is a periphery cell and will be modeled with a higher frequency than cell 1.

We will proceed by analyzing the FN equations to find for which values of α an oscillation exists, and how its frequency varies with α.

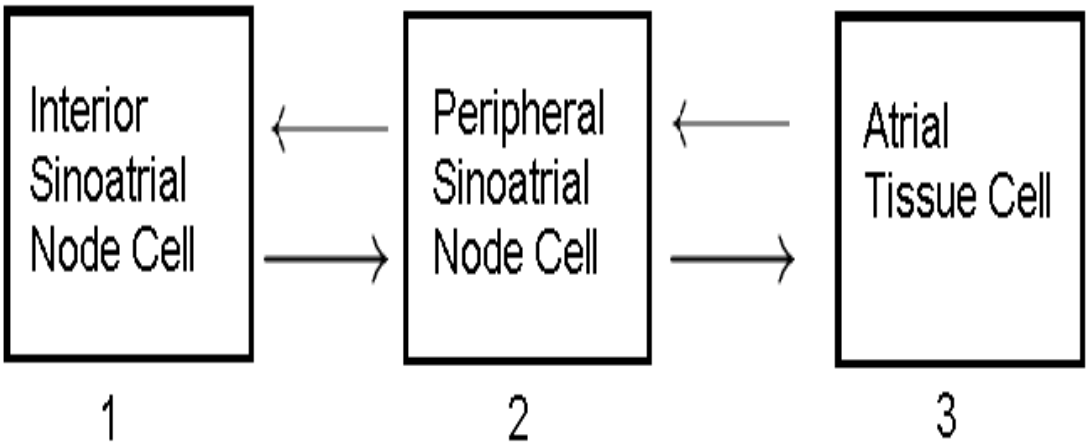

Figure 2.1: Three cell model

2.2 Analyses

To examine the FN equations we employ two types of analysis: exact and approximate. The exact analysis, which is local, valid in the neighborhood of an equilibrium point, will be used to classify the equilibria and to determine their stability and bifurcation. In addition, we will use an approximate analysis to study the relaxation oscillations which occur in eqs. (1) and (2). The approximate analysis consists of a fast-slow approximation which is based on the structure of eqs. (1) and (2) for small ϵ.

We will study the frequencies of oscillation in three ways: 1)Poincaré-Lindstedt, 2.)Fast-slow analysis, and 3.)Numerical simulation. We will use a Poincaré-Lindstedt perturbation analysis to find the frequencies of oscillation as a function of α. Next, this will be compared to oscillation frequencies obtained by using the fast-slow manifold approach. Finally, our results will be compared with those of numerical integration.

2.2.1 Exact Analysis

We begin our exact analysis by setting the right-hand side of equations (2.11) and (2.12) equal to zero in order to find equilibria:

$$\begin{aligned} \epsilon\dot{v} &= -v(v-\alpha)(v-1) - w = 0 \qquad (2.3) \\ &\Rightarrow \quad w = -v(v-\alpha)(v-1) \\ \dot{w} &= v - w = 0 \qquad (2.4) \\ &\Rightarrow \quad v = w \end{aligned}$$

Note that the origin, $v = w = 0$, is an equilibrium point for all α. Additional equilibria will correspond to real roots of

$$\begin{aligned} &(v-\alpha)(v-1) + 1 = 0 \\ &\Rightarrow v = \tfrac{(\alpha+1) \pm \sqrt{(\alpha-3)(\alpha+1)}}{2} \qquad (2.5) \end{aligned}$$

Thus, we find that there exist two additional equilibria for $\alpha < -1$ and $\alpha > 3$.

Next, we classify our equilibria using the Jacobian of equations (2.11) and (2.12).

$$J = \begin{bmatrix} \frac{\partial \dot{v}}{\partial v} & \frac{\partial \dot{v}}{\partial w} \\ \frac{\partial \dot{w}}{\partial v} & \frac{\partial \dot{w}}{\partial w} \end{bmatrix} = \begin{bmatrix} -\frac{1}{\epsilon}(3v^2 - 2(1+\alpha)v + \alpha) & 1 \\ -\frac{1}{\epsilon} & -1 \end{bmatrix} \qquad (2.6)$$

At the origin, $(v, w) = (0, 0)$

$$J_{(0,0)} = \begin{bmatrix} -\frac{\alpha}{\epsilon} & 1 \\ -\frac{1}{\epsilon} & -1 \end{bmatrix} \qquad (2.7)$$

The nature of the equilibrium point depends on the trace and determinant of J, see Fig. 2.

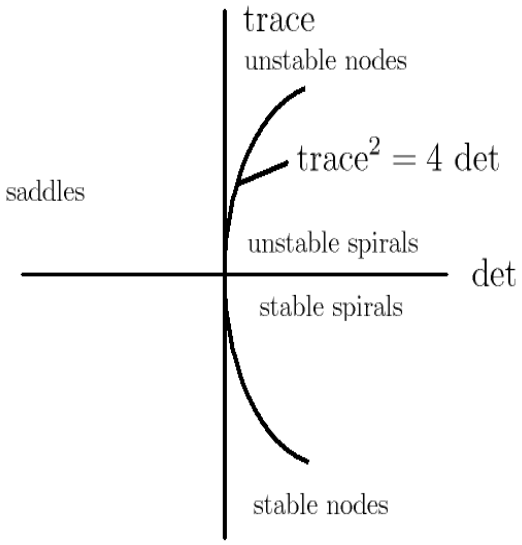

Figure 2.2: Stability diagram

From (2.7), the trace,

$$tr(J) = -\frac{\alpha}{\epsilon} - 1$$

and determinant,

$$det(J) = \frac{1}{\epsilon}(1 + \alpha)$$

For a stable equilibrium point, $tr(J) < 0$ and $det(J) > 0$. For $tr(J) < 0 \Rightarrow \alpha > -\epsilon$. For $det(J) > 0 \Rightarrow \alpha > -1$. So for $\alpha > -\epsilon$ the origin is a stable spiral or node (region II in Fig.3). Using Fig.2 we also see that for $-1 < \alpha < -\epsilon$ (region I) the origin is an unstable spiral or node.

For our model we would like to have two self-oscillatory cells. Mathematically, this means there will be limit cycles present in our analysis. In the $\alpha - \epsilon$ plane (Fig. 3) as we cross the line $\alpha = -\epsilon$ we find that a supercritical Hopf bifurcation occurs, thus giving us a stable limit cycle. We will show this later using Lindstedt's method. Thus we will choose the SA nodal cells (1 and 2 in Fig.1) to be located in region I of Fig.3. The atrial cell (3 in Fig.1) will be located in region II.

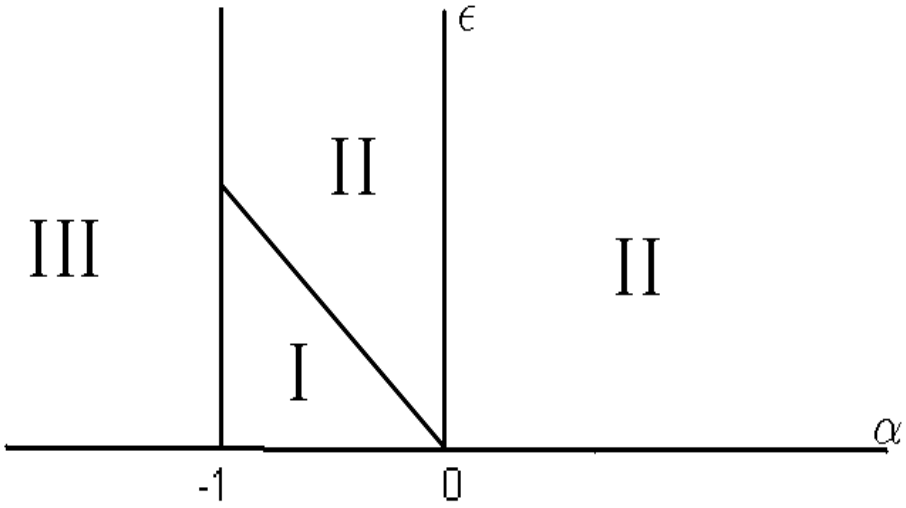

Figure 2.3: Results of exact local analysis of eqs. (1), (2) displayed in $\alpha - \epsilon$ plane. In region I the origin is an unstable spiral or node, while in region II the origin is stable. Systems in region I contain a stable limit cycle which is created via a supercritical Hopf as the line $\alpha = -\epsilon$ is crossed. In region III the origin is a saddle.

2.2.2 Approximate Analysis

The forgoing analysis of equilibria will now be supplemented with a fast-slow approximation which gives good approximations for the periodic motions (relaxation type limit cycles). In the limit as $\epsilon \to \infty$ (2.11) and (2.12) become

$$0 = -v(v-\alpha)(v-1) - w \tag{2.8}$$

$$\dot{w} = v - w \tag{2.9}$$

Solving (8) for w we get an equation for the slow manifold of the system.

$$w = -v(v-\alpha)(v-1) \tag{2.10}$$

This plots as a cubic which crosses the v-axis at $v = 0, \alpha, 1$ (Fig. 4).

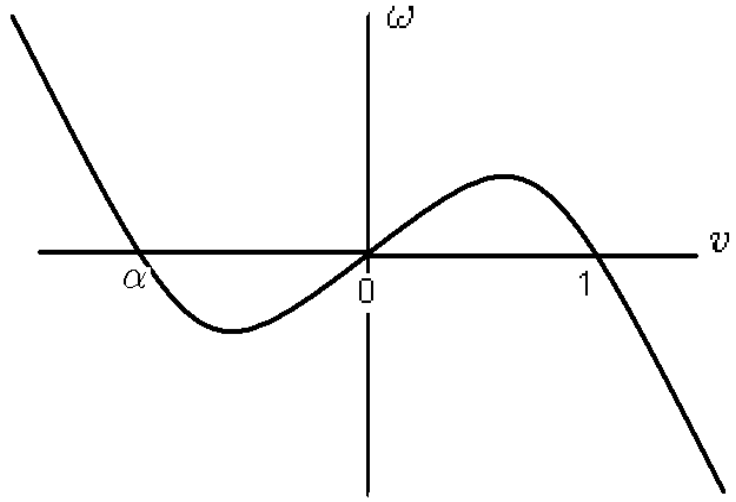

Figure 2.4: Slow manifold.

For $\epsilon > 0$, motions starting away from the slow manifold approach it on a fast time scale. The direction of flow is shown by arrows in Fig. 5. The slow manifold is stable from A to B and from C to D but is unstable from B to C.

$v = 0$ on the v-axis is an equilibrium point, and it turns out that its stability and the nature of the dynamics depends on whether $\alpha > 0$ or $\alpha < 0$. Since for

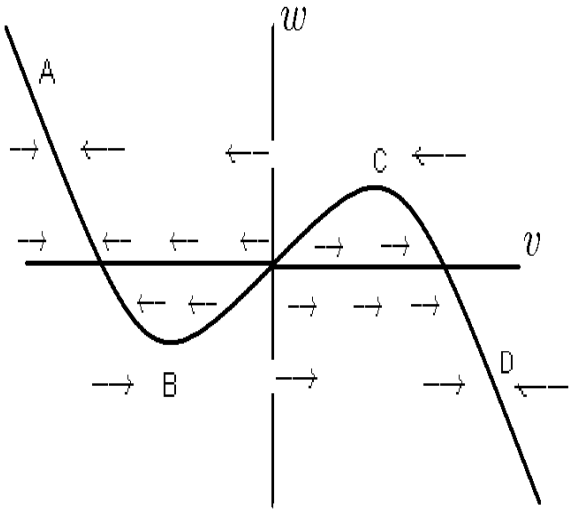

Figure 2.5: Slow manifold with vector fields

$\alpha > 0$ the equilibrium point at the origin lies on the stable portion of the slow manifold, no oscillation occurs. However for $\alpha < 0$, Fig. 6 shows that an oscillation occurs because the equilibrium at the origin lies on the unstable part of the slow manifold.

2.2.3 Exact Analysis vs. Approximate Analysis

In conclusion the fast-slow approximate analysis gives that eqs. (2.11) and (2.12) oscillate for $\alpha < 0$ whereas the exact analysis given in section 2.2 gives that an oscillation occurs for $\alpha < -\epsilon$. Since the fast-slow analysis assumes $\epsilon \ll 1$, there is not too much difference between these results. The fast-slow analysis is incorrect, but only by an amount that is $O(\epsilon)$.

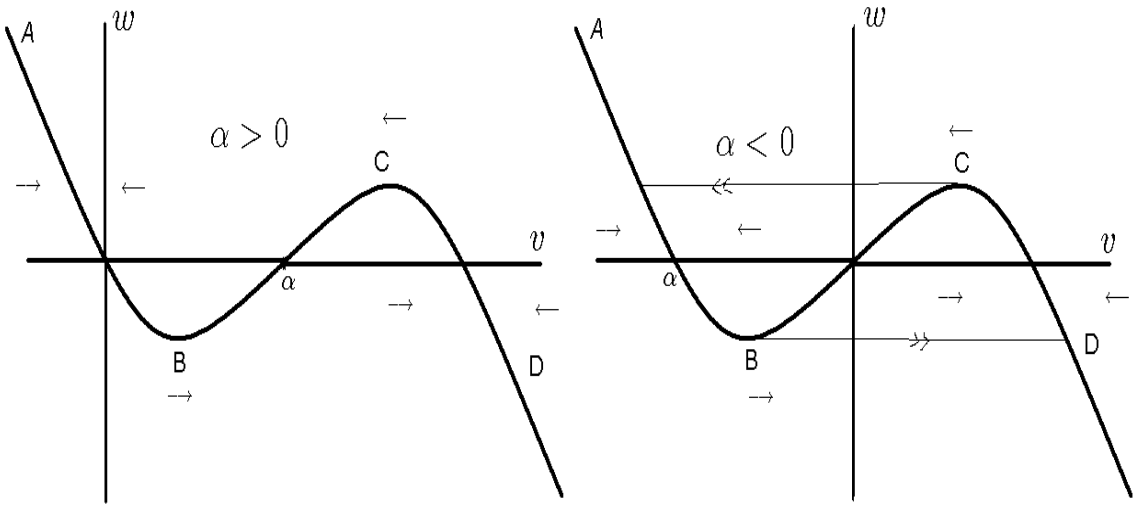

Figure 2.6: $\alpha > 0$ and $\alpha < 0$

2.3 Period of Oscillation

The cells of the SA node have different frequencies. In particular, the periphery cells have a higher frequency than the interior cells (Cai p.220). Thus, our next goal is to determine the frequency of oscillation as it varies with α. We will use Lindstedt method, fast-slow analysis, and numerical simulation.

2.3.1 Lindstedt Method

The Lindstedt method is good for approximating the relationship between period and amplitude in limit cycle oscillations. From the Fitzhugh-Nagumo equations (1),(2)

$$\epsilon \dot{v} = -v(v-\alpha)(v-1) - w \tag{2.11}$$

$$\dot{w} = v - w \tag{2.12}$$

we take the derivative of (12),

$$\ddot{w} = \dot{v} - \dot{w}$$

. Then we substitute the expression for $\dot{v}$ from (11) into the above $\ddot{w}$ equation. The resulting equation

$$\frac{d^2w}{dt^2} = \frac{-w - (v-1)\ v\ (v-\alpha)}{\epsilon} - \frac{dw}{dt} \tag{2.13}$$

depends on v, w, and $\dot{w}$. From (12), $v = \dot{w} + w$. Thus (13) becomes

$$\begin{aligned}\frac{d^2w}{dt^2} \quad = \quad & -\frac{\left(\frac{dw}{dt}\right)^3}{\epsilon} - \frac{3\,w\,\left(\frac{dw}{dt}\right)^2}{\epsilon} + \frac{\alpha\,\left(\frac{dw}{dt}\right)^2}{\epsilon} + \frac{\left(\frac{dw}{dt}\right)^2}{\epsilon} - \frac{3\,w^2\,\frac{dw}{dt}}{\epsilon} + \frac{2\,\alpha\,w\,\frac{dw}{dt}}{\epsilon} + \\ & \frac{2\,w\,\frac{dw}{dt}}{\epsilon} - \frac{\alpha\,\frac{dw}{dt}}{\epsilon} - \frac{dw}{dt} - \frac{w^3}{\epsilon} + \frac{\alpha\,w^2}{\epsilon} + \frac{w^2}{\epsilon} - \frac{\alpha\,w}{\epsilon} - \frac{w}{\epsilon}\end{aligned} \tag{2.14}$$

We have now reduced the two FN equations to one second order differential equation that depends only on w and $\frac{dw}{dt}$.

We learned from our exact analysis in Sec. 2.1 that a Hopf bifurcation occurs for $\alpha = -\epsilon$. Thus, we perturb a value, μ, from this point to understand what happens in the neighborhood of this point. We set $\alpha = -\epsilon + \mu$. For a limit cycle we expect $\mu < 0$. We also find the linear terms containing w in (14) and subtract them from both sides. The resulting equation is

$$\begin{aligned}\frac{d^2w}{dt^2} + (\frac{\mu}{\epsilon} + \frac{1}{\epsilon} - 1)w + \frac{\mu}{\epsilon}\frac{dw}{dt} = & -\frac{\left(\frac{dw}{dt}\right)^3}{\epsilon} - \frac{3\,w\,\left(\frac{dw}{dt}\right)^2}{\epsilon} + \frac{\mu\,\left(\frac{dw}{dt}\right)^2}{\epsilon} \\ + \frac{\left(\frac{dw}{dt}\right)^2}{\epsilon} - \left(\frac{dw}{dt}\right)^2 - \frac{3\,w^2\,\frac{dw}{dt}}{\epsilon} + \frac{2\,\mu\,w\,\frac{dw}{dt}}{\epsilon} + \frac{2\,w\,\frac{dw}{dt}}{\epsilon} - 2\,w\,\frac{dw}{dt} - \frac{w^3}{\epsilon} & \\ + \frac{\mu\,w^2}{\epsilon} + \frac{w^2}{\epsilon} - w^2 & \end{aligned} \tag{2.15}$$

We replace t by a new independent variable $z = \sqrt{\frac{\mu}{\epsilon} + \frac{1}{\epsilon} - 1}\ t$ so that eq.(14) has a linear undamped frequency of 1. Since $\frac{dw}{dt} = \frac{dw}{dz}\frac{dz}{dt}$,(15) becomes

$$\begin{aligned} \frac{d^2w}{dz^2} + c\frac{dw}{dz} + w &= a_1w^2 + a_2w\frac{dw}{dz} + a_3(\frac{dw}{dz})^2 + b_1w^3 \\ &+ b_2w^2\frac{dw}{dz} + b_3w(\frac{dw}{dz})^2 + b_4(\frac{dw}{dz})^3 + \cdots \end{aligned} \tag{2.16}$$

where

$$c = \frac{\mu}{\sqrt{\epsilon}\sqrt{\mu - \epsilon + 1}} \tag{2.17}$$

$$a_1 = -1 \tag{2.18}$$

$$a_2 = -\frac{2\sqrt{\mu - \epsilon + 1}}{\sqrt{\epsilon}} \tag{2.19}$$

$$a_3 = \frac{\mu - \epsilon + 1}{\epsilon} \tag{2.20}$$

$$b_1 = \frac{\epsilon}{\epsilon\mu - \epsilon^2 + \epsilon} \tag{2.21}$$

$$b_2 = \frac{3}{\sqrt{\epsilon}\sqrt{\mu - \epsilon + 1}} \tag{2.22}$$

$$b_3 = \frac{3}{\epsilon} \tag{2.23}$$

$$b_4 = \frac{\sqrt{\mu - \epsilon + 1}}{\epsilon^{\frac{3}{2}}} \tag{2.24}$$

From (Rand and Armbuster p.23), we simplify (16) and find the following expression obtained via Lindstedt's method for the frequency as it depends on α and ϵ. Here we have set $\mu = \alpha + \epsilon$

$$frequency = -\frac{10\,\alpha\,\epsilon^2 + \epsilon^2 + 2\,\alpha^2\,\epsilon + 3\,\alpha\,\epsilon + 10\,\epsilon + 4\,\alpha^3 + 8\,\alpha^2 + 4\,\alpha}{6\ (\alpha + 1)\ (2\,\alpha - 1)\ \epsilon} \tag{2.25}$$

At $\alpha = -\epsilon$ there is a Hopf bifurcation and we have $\mu = 0$. We replace z with t by saying $t = (\frac{\alpha+\epsilon}{\epsilon} + \frac{1}{\epsilon} - 1)^{-\frac{1}{2}}z = (\frac{\alpha+1}{\epsilon})^{-\frac{1}{2}}z$. Using $period = \frac{2\pi}{frequency}$ and

substituting t we have the following equation and resulting plot of period vs. α in Fig. 7.

$$period = \frac{2\pi(6\ (\alpha+1)\ (2\,\alpha-1)\ \epsilon}{(\sqrt{\frac{\alpha+1}{\epsilon}})(-10\,\alpha\,\epsilon^2-\epsilon^2-2\,\alpha^2\,\epsilon-3\,\alpha\,\epsilon-10\,\epsilon-4\,\alpha^3-8\,\alpha^2-4\,\alpha)} \quad (2.26)$$

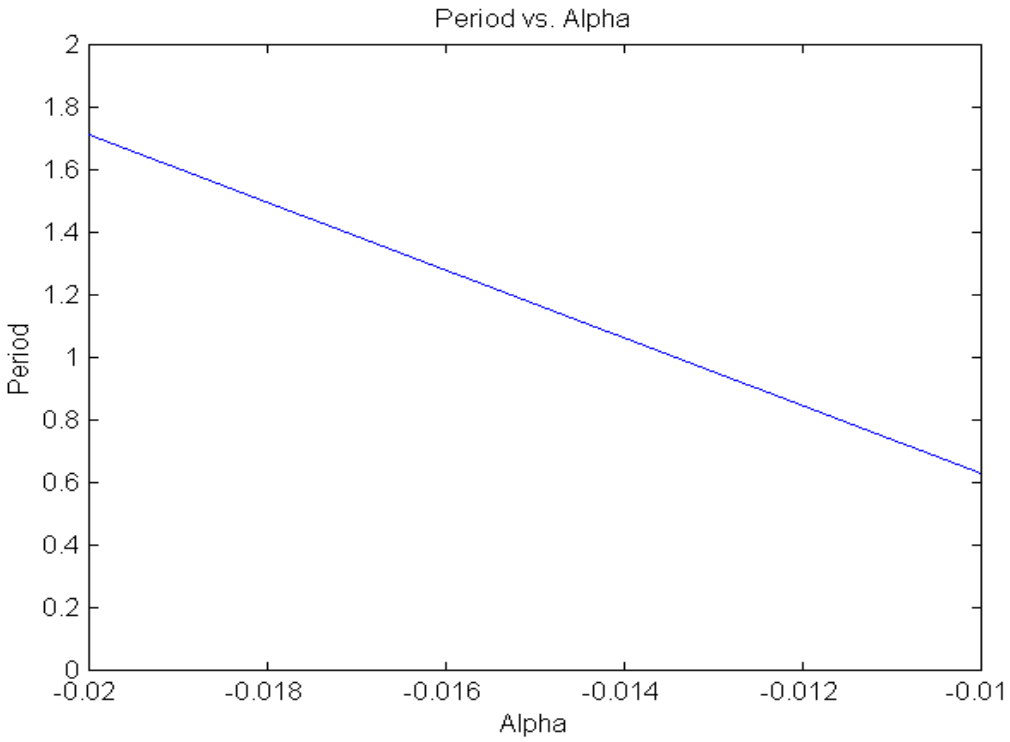

Figure 2.7: Graph of period vs. α resulting from Lindstedt analysis.(ϵ = 0.01)

2.3.2 Fast-Slow Analysis

In the case $\alpha < 0$ we find that there exists a limit cycle (Fig.8). The limit cycle consists of four pieces: $A \rightarrow B$, $B \rightarrow D$,$D \rightarrow C$, and $C \rightarrow A$. Because ϵ is so small the horizontal motions from $B \rightarrow D$ and $C \rightarrow A$ are so fast that we neglect the time it takes to travel between the points. The expression for the period will

therefore be the sum of the time it takes to get from $A \to B$ and from $D \to C$. To determine these times we first obtain expressions for the location of the points A, B, C, D. At B and C the slope of the slow manifold is zero which implies that $\frac{dw}{dv} = 0$ at those points. B and C lie on the slow manifold, $w = -v(v-\alpha)(v-1)$. So,

$$\begin{aligned} \frac{dw}{dv} &= -3v^2 + 2\alpha v + 2v - \alpha = 0 \Rightarrow & (2.27) \\ v_C &= \frac{\sqrt{\alpha^2 - \alpha + 1}}{3} + \frac{\alpha}{3} + \frac{1}{3} & (2.28) \\ v_B &= -\frac{\sqrt{\alpha^2 - \alpha + 1}}{3} + \frac{\alpha}{3} + \frac{1}{3} & (2.29) \end{aligned}$$

From Fig. 8 we see that C has the same w value as A, hence from (10) $w_A = w_C = -v_C(v_C - \alpha)(v_C - 1)$. In order to find v_A, we substitute w_A into eq. (10):

$$w_A = -v_A(v_A - \alpha)(v_A - 1). \tag{2.30}$$

Solving (14) for v_A gives

$$v_A = \frac{-2\sqrt{\alpha^2 - \alpha + 1}}{3} + \frac{\alpha}{3} + \frac{1}{3} \tag{2.31}$$

Similarly for D we get

$$v_D = \frac{2\sqrt{\alpha^2 - \alpha + 1}}{3} + \frac{\alpha}{3} + \frac{1}{3} \tag{2.32}$$

We would now like to find the time it takes to get from $A \to B$. From (10),(11)

$$w = -v(v-\alpha)(v-1) \Rightarrow \tag{2.33}$$

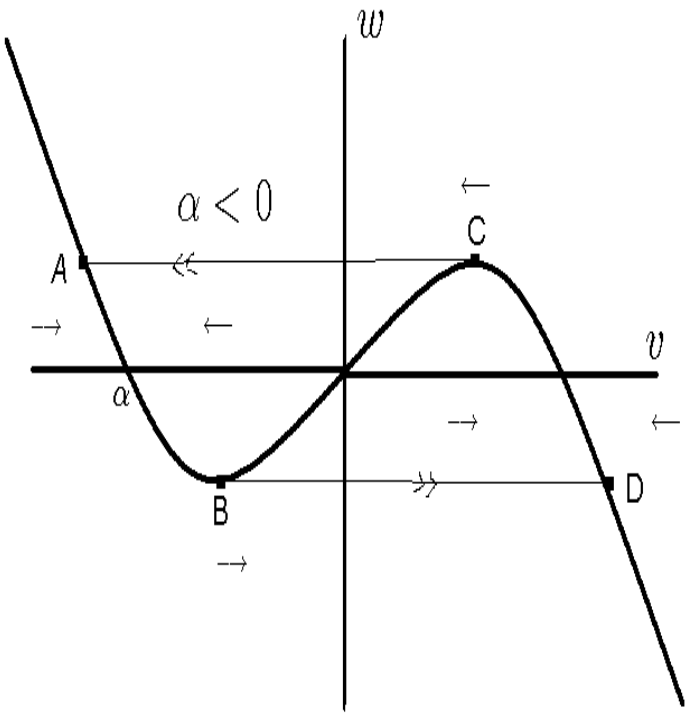

Figure 2.8: For $\alpha < 0$ there is a limit cycle. A to B and D to C are the segments of slow flow. B to D and C to A are segments of fast flow on the limit cycle.

$$\dot{w} = \frac{dw}{dv}\dot{v} = (-3v^2 + 2\alpha v + 2v - \alpha)\dot{v} \tag{2.34}$$

From (9), $\dot{w} = v - w$. We set the right-hand side of (9) equal to the right-hand side of (18) and solve for $\dot{v}$. Using (10) we get

$$\frac{dv}{dt} = -\frac{v(v^2 - \alpha v_v + \alpha)}{3v^2 - 2\alpha v - 2v + \alpha} \tag{2.35}$$

Solving (19) using Macsyma we obtain

$$t = g(v) + K$$

where $g(v)$ is a complicated function of v and K is an arbitrary constant of integration. To find the time spent between points A and B, we write

$$t_A = g(v_A) + K \tag{2.36}$$

$$t_B = g(v_B) + K \tag{2.37}$$

Subtracting we get $t_B - t_A = g(v_B) - g(v_A)$. Similarly we obtain $t_C - t_D = g(v_C) - g(v_B)$. Adding these two travel times, we obtain the following expression for the period of oscillation:

$$period = (t_B - t_A) + (t_C - t_D) = \tag{2.38}$$

$$-\frac{2\sqrt{-\alpha^2+2\alpha+3}\,\arctan\left(\frac{4\sqrt{\alpha^2-\alpha+1}}{3\sqrt{-\alpha^2+2\alpha+3}}+\frac{\alpha}{3\sqrt{-\alpha^2+2\alpha+3}}+\frac{1}{3\sqrt{-\alpha^2+2\alpha+3}}\right)}{2\alpha^2-4\alpha-6}$$

$$+\frac{2\sqrt{-\alpha^2+2\alpha+3}\,\arctan\left(\frac{4\sqrt{\alpha^2-\alpha+1}}{3\sqrt{-\alpha^2+2\alpha+3}}-\frac{\alpha}{3\sqrt{-\alpha^2+2\alpha+3}}-\frac{1}{3\sqrt{-\alpha^2+2\alpha+3}}\right)}{2\alpha^2-4\alpha-6}$$

$$+\frac{2\sqrt{-\alpha^2+2\alpha+3}\,\arctan\left(\frac{2\sqrt{\alpha^2-\alpha+1}}{3\sqrt{-\alpha^2+2\alpha+3}}+\frac{\alpha}{3\sqrt{-\alpha^2+2\alpha+3}}+\frac{1}{3\sqrt{-\alpha^2+2\alpha+3}}\right)}{2\alpha^2-4\alpha-6}$$

$$-\frac{2\sqrt{-\alpha^2+2\alpha+3}\,\arctan\left(\frac{2\sqrt{\alpha^2-\alpha+1}}{3\sqrt{-\alpha^2+2\alpha+3}}-\frac{\alpha}{3\sqrt{-\alpha^2+2\alpha+3}}-\frac{1}{3\sqrt{-\alpha^2+2\alpha+3}}\right)}{2\alpha^2-4\alpha-6}$$

$$+\frac{2\alpha^2\,\log\left(2\alpha\sqrt{\alpha^2-\alpha+1}+2\sqrt{\alpha^2-\alpha+1}+2\alpha^2+\alpha+11\right)}{2\alpha^2-4\alpha-6}$$

$$-\frac{3\alpha\,\log\left(2\alpha\sqrt{\alpha^2-\alpha+1}+2\sqrt{\alpha^2-\alpha+1}+2\alpha^2+\alpha+11\right)}{2\alpha^2-4\alpha-6}$$

$$-\frac{9\,\log\left(2\alpha\sqrt{\alpha^2-\alpha+1}+2\sqrt{\alpha^2-\alpha+1}+2\alpha^2+\alpha+11\right)}{2\alpha^2-4\alpha-6}$$

$$-\frac{2\alpha^2\,\log\left(\alpha\sqrt{\alpha^2-\alpha+1}+\sqrt{\alpha^2-\alpha+1}-\alpha^2+4\alpha+8\right)}{2\alpha^2-4\alpha-6}$$

$$+\frac{3\alpha\,\log\left(\alpha\sqrt{\alpha^2-\alpha+1}+\sqrt{\alpha^2-\alpha+1}-\alpha^2+4\alpha+8\right)}{2\alpha^2-4\alpha-6}$$

$$+\frac{9\,\log\left(\alpha\,\sqrt{\alpha^2-\alpha+1}+\sqrt{\alpha^2-\alpha+1}-\alpha^2+4\,\alpha+8\right)}{2\,\alpha^2-4\,\alpha-6}$$
$$-\frac{2\,\alpha^2\,\log\left(-\alpha\,\sqrt{\alpha^2-\alpha+1}-\sqrt{\alpha^2-\alpha+1}-\alpha^2+4\,\alpha+8\right)}{2\,\alpha^2-4\,\alpha-6}$$
$$+\frac{3\,\alpha\,\log\left(-\alpha\,\sqrt{\alpha^2-\alpha+1}-\sqrt{\alpha^2-\alpha+1}-\alpha^2+4\,\alpha+8\right)}{2\,\alpha^2-4\,\alpha-6}$$
$$+\frac{9\,\log\left(-\alpha\,\sqrt{\alpha^2-\alpha+1}-\sqrt{\alpha^2-\alpha+1}-\alpha^2+4\,\alpha+8\right)}{2\,\alpha^2-4\,\alpha-6}$$
$$+\frac{2\,\alpha^2\,\log\left(-2\,\alpha\,\sqrt{\alpha^2-\alpha+1}-2\,\sqrt{\alpha^2-\alpha+1}+2\,\alpha^2+\alpha+11\right)}{2\,\alpha^2-4\,\alpha-6}$$
$$-\frac{3\,\alpha\,\log\left(-2\,\alpha\,\sqrt{\alpha^2-\alpha+1}-2\,\sqrt{\alpha^2-\alpha+1}+2\,\alpha^2+\alpha+11\right)}{2\,\alpha^2-4\,\alpha-6}$$
$$-\frac{9\,\log\left(-2\,\alpha\,\sqrt{\alpha^2-\alpha+1}-2\,\sqrt{\alpha^2-\alpha+1}+2\,\alpha^2+\alpha+11\right)}{2\,\alpha^2-4\,\alpha-6}$$
$$+\frac{2\,\alpha^2\,\log\left(2\,\sqrt{\alpha^2-\alpha+1}+\alpha+1\right)}{2\,\alpha^2-4\,\alpha-6}$$
$$-\frac{6\,\alpha\,\log\left(2\,\sqrt{\alpha^2-\alpha+1}+\alpha+1\right)}{2\,\alpha^2-4\,\alpha-6}$$
$$-\frac{2\,\alpha^2\,\log\left(\sqrt{\alpha^2-\alpha+1}+\alpha+1\right)}{2\,\alpha^2-4\,\alpha-6}$$
$$+\frac{6\,\alpha\,\log\left(\sqrt{\alpha^2-\alpha+1}+\alpha+1\right)}{2\,\alpha^2-4\,\alpha-6}$$
$$-\frac{2\,\alpha^2\,\log\left(-\sqrt{\alpha^2-\alpha+1}+\alpha+1\right)}{2\,\alpha^2-4\,\alpha-6}$$
$$+\frac{6\,\alpha\,\log\left(-\sqrt{\alpha^2-\alpha+1}+\alpha+1\right)}{2\,\alpha^2-4\,\alpha-6}$$
$$+\frac{2\,\alpha^2\,\log\left(-2\,\sqrt{\alpha^2-\alpha+1}+\alpha+1\right)}{2\,\alpha^2-4\,\alpha-6}$$
$$-\frac{6\,\alpha\,\log\left(-2\,\sqrt{\alpha^2-\alpha+1}+\alpha+1\right)}{2\,\alpha^2-4\,\alpha-6}$$

See Fig. 8 where eq.(37) is plotted showing period as a function of α.

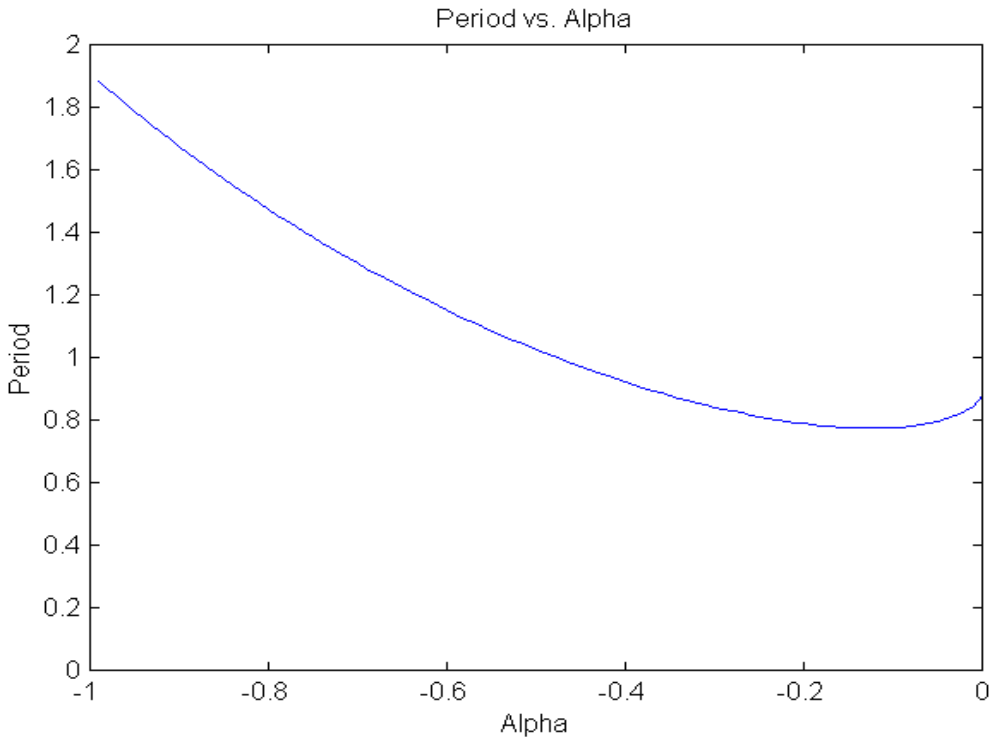

Figure 2.9: Graph of period vs. α resulting from fast-slow analysis.($\epsilon = 0.01$)

2.3.3 Numerical Simulation

We compare the results of Lindstedt's method, Fig.8, and the Fast-Slow approximation, Fig.9, on one graph Fig.10. (Note: $\epsilon = 0.01$ in all figures). From Fig. 10 we note that the two methods do not agree. The fast-slow analysis incorrectly predicts that the limit cycle exists in the small region $-0.01 < \alpha < 0$. The Lindstedt analysis corrects this defect but is only valid near the Hopf bifurcation, i.e. for $-0.012 < \alpha < -0.010$. To check these analyses we also used numerical simulation. Using Matlab we employed a Runge-Kutta order 4 algorithm and plotted the results shown in Figs. 11 and 12. From Fig. 11 we see that the numerical integration approximately agrees with the Fast-Slow approximation of limit cycle for values of α from -0.8 to -0.2. At $\alpha \approx -0.1$ there is a kink in the graph of limit cycle period

as determined by numerical simulation. The source of this feature has been traced to a sudden change in the size of the limit cycle. Using a numerical integration program called pplane5 in Matlab, we found that for $\alpha = -0.01282$ (Fig.13) a small limit cycle is present whereas for $\alpha = -0.01283$ (Fig.14) a much larger limit cycle appears. In conclusion, for $\epsilon = 0.01$, Fig.11 shows that the fast-slow analysis is unusable for $\alpha > -0.1$.

Fig.12 shows that Lindstedt's method is only valid for α close to -.01($= -\epsilon$). In future work we plan to use the fast-slow approximation for our model of 3 oscillators (see Fig.1), choosing $\alpha_1, \alpha_2 < -0.1$ (where the fast-slow approximation works best). We will also use the fast-slow approximation for the third Fitzhugh-Nagumo unit (modeling non-oscillatory atrial tissue) with $\alpha_3 > 0$.

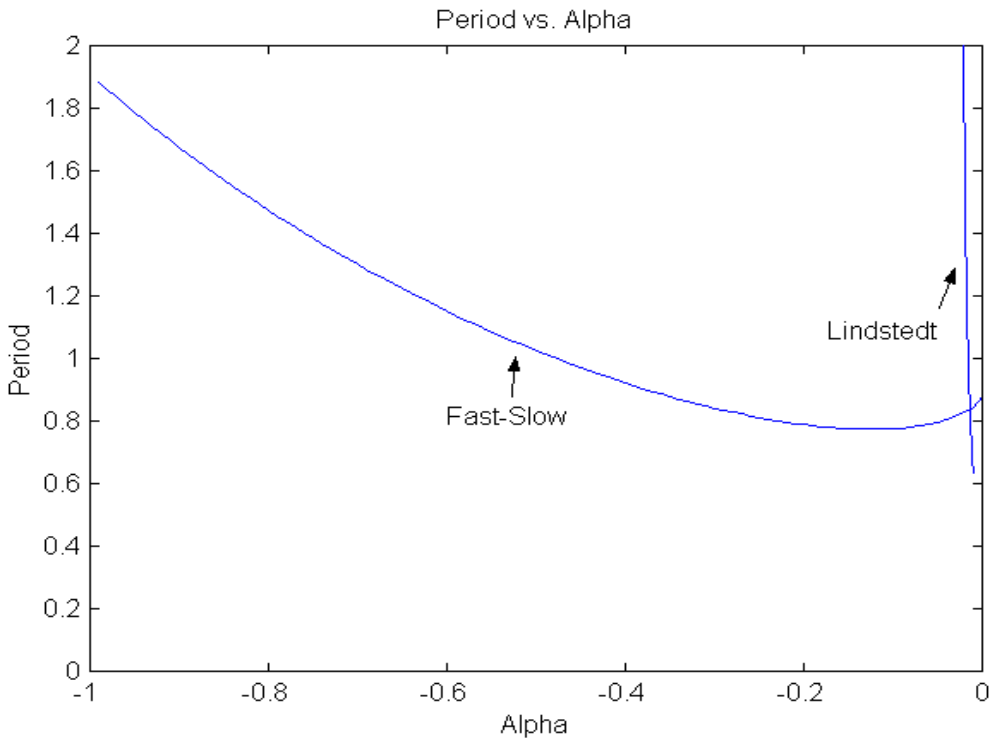

Figure 2.10: Graph of period vs. α resulting from fast-slow analysis and Lindstedt's method.($\epsilon = 0.01$)

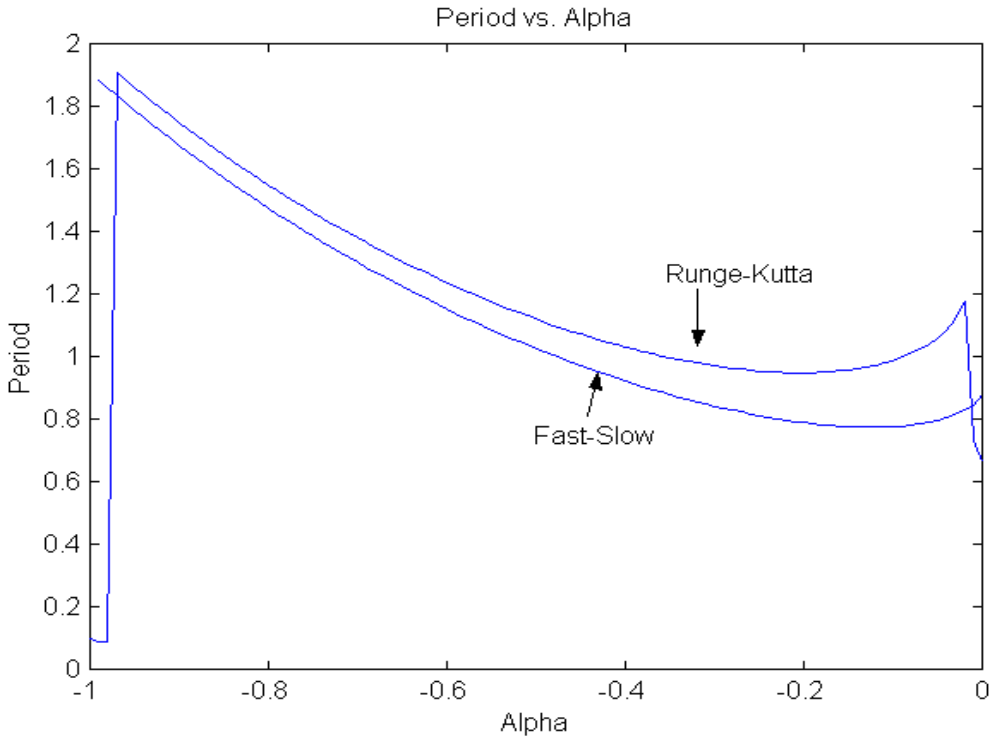

Figure 2.11: Graph of period vs. α Runge-Kutta and Fast-Slow methods compared.($\epsilon = 0.01$)

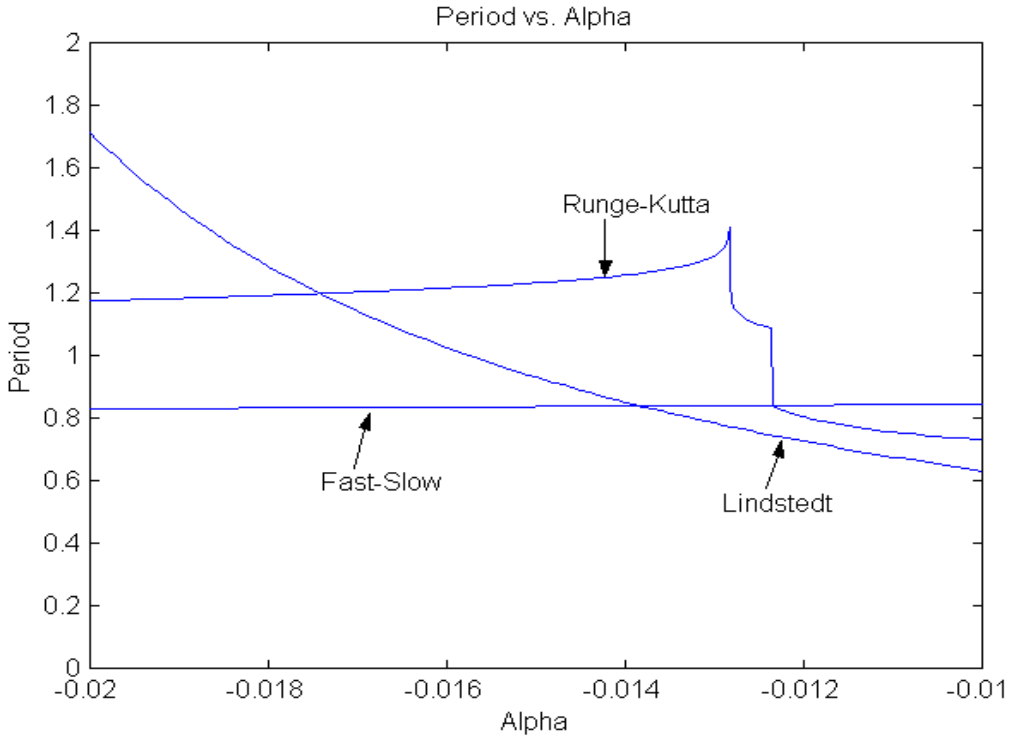

Figure 2.12: Graph of period vs. α Runge-Kutta, Fast-Slow, and Lindstedt methods compared.($\epsilon = 0.01$)

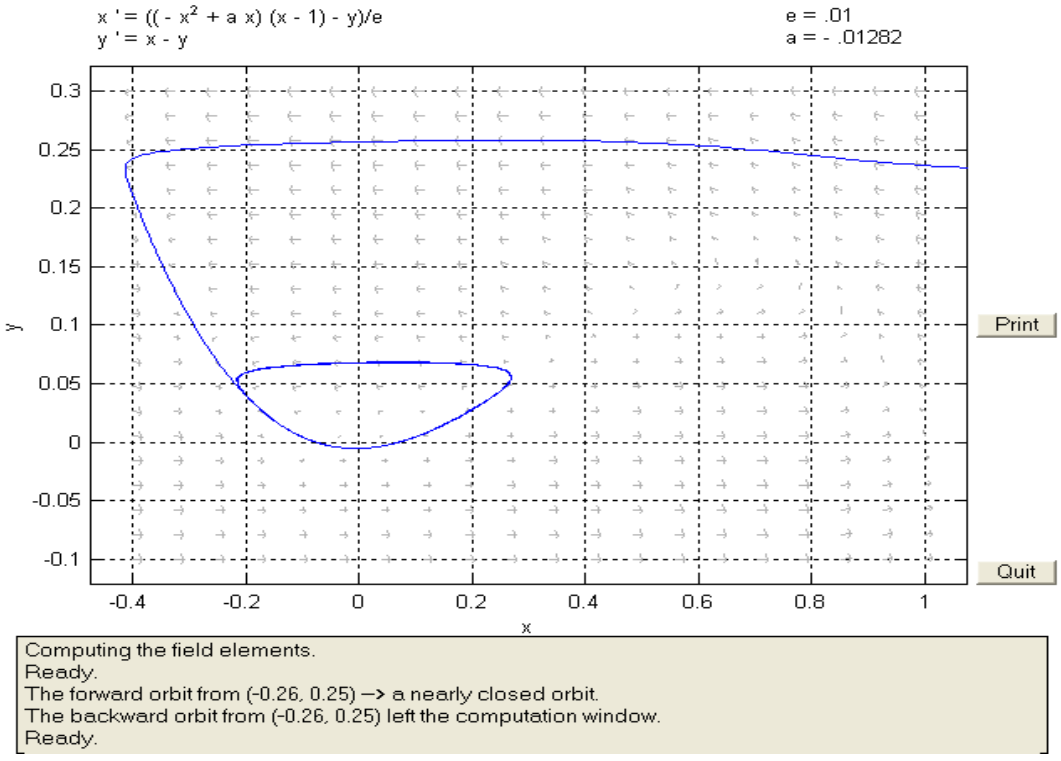

Figure 2.13: Small limit cycle produced at $\alpha = -0.01282$)

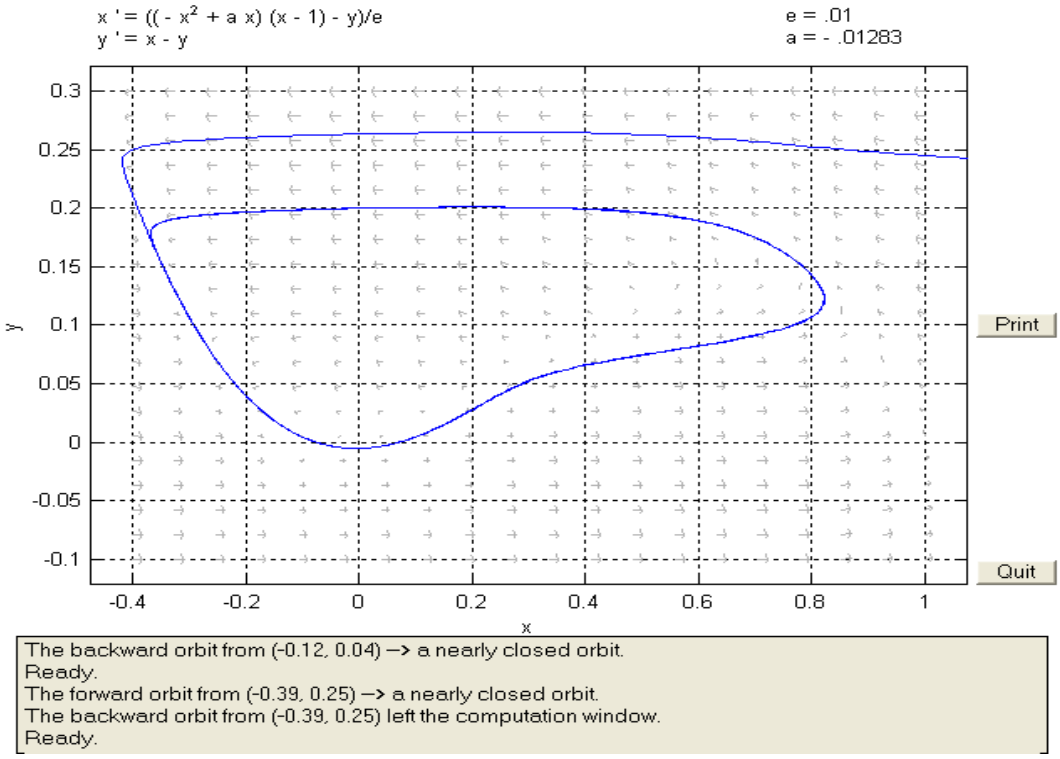

Figure 2.14: Large limit cycle produced at $\alpha = -0.01283$)

BIBLIOGRAPHY

Armbruster, Dieter and Rand, Richard H. Perturbation Methods, Bifurcation Theory, and Computer Algebra. Published: New York : Springer-Verlag, 1987.

Bretscher, Otto. Linear Algebra with Applications, 2nd ed. Published: New Jersey : Prentice Hall, 2001

D. Cai, R. L. Winslow, D. Noble. "Effects of Gap Junction Conductance on Dynamics of Sinoatrial Node Cells: Two-Cell and Large-Scale Network Models". IEEE Transactions on Biomedical Engineering, vol. 41, no. 3, March 1994.

Keener, James and Sneyd, James. Mathematical Physiology. New York: Springer-Verlag, 1998.

Macsyma Front End. ver 2.1.5 for ver 2.1. Macsyma Inc., 1994-96.

MATLAB. ver 5.3.0.10183(R11). The Mathworks Inc., 1984-99.

pplane5. ODE Software for Matlab. http://math.rice.edu/ polking/odesoft/dfpp.html

Sinoatrial Node. http://biology.about.com/library/organs/heart/blsinoatrialnode.htm.

Strogatz, Steven H. Nonlinear Dynamics and Chaos with Applications

in Physics, Biology, Chemistry, and Engineering. Reading, Mass. Addison-Wesley Pub, 1994.